Atmos. Chem. Phys. Discuss., 10, 28057–28107, 2010
www.atmos-chem-phys-discuss.net/10/28057/2010/
doi:10.5194/acpd-10-28057-2010

Atmospheric Chemistry and Physics Discussions

Simple kinematic models for the environmental interaction of tropical cyclones in vertical wind shear

M. Riemer[1] **and M. T. Montgomery**[1,2]

[1]Department of Meteorology, Naval Postgraduate School, Monterey, CA, USA
[2]NOAA's Hurricane Research Division, Miami, FL, USA

Received: 28 August 2010 – Accepted: 8 October 2010 – Published: 16 November 2010

Correspondence to: M. Riemer (mriemer@uni-mainz.de)

Published by Copernicus Publications on behalf of the European Geosciences Union.

Abstract

A major contribution to intensity changes of tropical cyclones (TCs) is believed to be associated with interaction with dry environmental air. However, the conditions under which pronounced TC-environment interaction takes place are not well understood. As a step towards improving our understanding of this problem we analyze the flow topology of a TC in vertical wind shear in an idealized, three-dimensional, convection-permitting numerical experiment. A set of distinct streamlines, the so-called separatrices, can be identified under the assumptions of steady and layer-wise horizontal flow. The separatrices are shown to divide the flow around the TC into distinct regions.

The separatrix structure in our numerical experiment is more complex than the well-known flow topology of a non-divergent point vortex in uniform background flow. In particular, one separatrix spirals inwards and ends in a limit cycle, a meso-scale dividing streamline encompassing the eyewall above the inflow and below the outflow layer. Air with the highest values of moist entropy resides within this limit cycle supporting the notion that the eyewall is well protected from intrusion of dry environmental air despite the adverse impact of the vertical wind shear. This "moist envelope" is distorted considerably by the vertical wind shear, and the shape of the moist envelope is closely related to the shape of the limit cycle.

A simple kinematic model based on a weakly divergent point vortex in background flow is presented. The model is shown to capture the essence of many salient features of the flow topology in the idealized experiment. A regime diagram representing realistic values of TC intensity and vertical wind shear can be constructed for this simple model. The results indicate distinct scenarios of environmental interaction depending on the ratio of storm intensity and shear magnitude. Further implications of the new results derived from the flow topology analysis for TCs in the real atmosphere are discussed.

ACPD

10, 28057–28107, 2010

1 Introduction

1.1 Tropical cyclone intensity and environmental air interaction

It has long been recognized that the interaction of tropical cyclones (TCs) with environmental air can have a detrimental effect on storm intensity. The interaction can be expected to be particularly pronounced when vertical shear of the environmental horizontal wind is present. Vertical wind shear ensures that at some height levels the environmental flow is distinct from the motion of the storm and considerable storm-relative environmental flow arises at such levels (e.g. Willoughby et al., 1984; Marks et al., 1992; Bender, 1997). This storm-relative flow then advects environmental air towards the TC. If low moist entropy air associated with the environment can intrude into the eyewall updrafts, then the conversion of heat into kinetic energy within the TC's power engine is frustrated and the storm can be expected to weaken (Tang and Emanuel, 2010a). Moistening and warming of the environmental air before reaching the eyewall updrafts may diminish this detrimental impact on TC intensity.

Simpson and Riehl (1958) were the first to propose that storm-relative flow "may act as a constraint upon the hurricane heat engine". Based on the inspection of the storm-relative radial flow at mid-levels (their Fig. 4), they noted "a prominent movement of environmental air through the storm" and suggested that "the vortex was *ventilated* by invading colder masses of air". This ventilation of the TC vortex by storm-relative flow is widely invoked to explain the intensity evolution of observed storms (e.g. Willoughby et al., 1984; Marks et al., 1992; Shelton and Molinari, 2009). Emanuel et al. (2004) developed an empirical parameterization that attempts to account for the ventilation of low entropy through the TC core at mid levels to include the effects of environmental vertical wind shear in an axisymmetric model[1]. A somewhat related pathway of environmental interaction in vertical shear was proposed by Frank and Ritchie (2001). In their model, shear-induced eddy fluxes of potential temperature may erode the upper-

[1]This empirical parameterization is now used every hurricane season in the CHIPS forecast model of Kerry Emanuel.

ACPD
10, 28057–28107, 2010

level warm core, leading to an increase of the minimum surface pressure by hydrostatic arguments, and thus to a decrease of TC intensity.

When considering TC-environment interaction it needs to be borne in mind that a mature TC constitutes a strong atmospheric vortex. This is particularly true when trying to draw conclusions from the *asymmetric* storm-relative flow, i.e. the storm-relative flow from which the axisymmetric TC circulation has been subtracted. The strong swirling winds significantly deflect the asymmetric storm-relative flow[2]. Air parcel trajectories in a mature TC, of course, differ greatly from the streamlines of the asymmetric storm-relative flow. This distinction does not always seem to be clear in a number of previous studies. The asymmetric storm-relative flow is sometimes referred to as "cross-vortex flow" (Willoughby et al., 1984; Black et al., 2002) or there is the tacit assumption that air flows *through* the inner core (Simpson and Riehl, 1958; Bender, 1997; Zhang and Kieu, 2006). Only for relatively weak storms and strong relative flow, however, does it seem plausible that environmental air will actually penetrate the eyewall of a TC (e.g. Hurricane Claudette (2003), Shelton and Molinari, 2009). The focus of this paper is to explore the limitations of vortex-environment interaction based on the foregoing purely kinematic considerations.

The foregoing ideas hint that a more efficient way to ingest dry environmental air into the eyewall updrafts is through the storm's inflow layer. Riemer et al. (2010, RMN hereafter) have shown how the interaction of vertical shear with a mature TC can form persistent, vortex-scale downdrafts which act to flush the inflow layer with low moist entropy (or equivalent potential temperature, θ_e) air and effectively reduce eyewall θ_e values by 3 K to 9 K, depending on the magnitude of vertical shear. Without explicit consideration of vertical shear effects, earlier studies have shown that downdrafts

[2]Furthermore, the strong radial shear of the swirling winds tends to damp any asymmetry that tries to invade the TC. This is the so-called vortex axisymmetrization process (Melander et al., 1987; Carr and Williams, 1989) that is a well known essential ingredient in the robustness and persistence of coherent vortex structures in quasi two-dimensional flows. This process, however, will not be considered explicitly in this study.

ACPD
10, 28057–28107, 2010

associated with individual rain bands may bring low θ_e air into the inflow layer (Barnes et al., 1983; Powell, 1990). Powell has estimated that the replenishment of this air by surface fluxes may not be complete before reaching the eyewall and concluded that this process could affect the intensity evolution of the storm. In a more recent modeling study, Kimball (2006) has found that "dry environmental air above approximately 850 hPa rotates cyclonically and inward around the storm center" and may be subsequently involved in downdrafts close to the eyewall. Two schematic diagrams summarizing how the TC power engine may be frustrated by mid-level ventilation and pronounced downdrafts are given in Figs. 1 and 2 of RMN.

The processes discussed above, the ventilation of eyewall convection, the erosion of the upper-level warm core, and the depression of inflow layer θ_e by downdrafts, are widely believed to operate in real storms. The relative importance of these processes for intensity modification is not well known and the environmental conditions under which they may operate are not well understood. This is partly reflected by the fact that the interaction with vertical shear and/or the presence of dry air in the vicinity of a storm poses an enhanced forecast challenge. Dry air can be observed to *impinge* on TCs (e.g. Zipser et al., 2009, tropical storm Debby), yet it has not been entirely clear how storm intensity is affected. Idealized experiments demonstrate that dry air may wrap all around a developing TC in quiescent environment without affecting storm intensity at all (S. A. Braun, personal communication, 2010). Similar questions arise for TCs that interact with the Saharan air layer (SAL)[3].

Aspects of TC-environment interaction have received considerable attention on the convective scale and the scale of individual rain bands (e.g. The Hurricane Rainband and Intensity Change Experiment, Houze et al., 2006). We believe, however, that an overarching framework for this problem is still lacking. The goal of the present study is to contribute to such a framework by taking a broader-scale viewpoint and considering the larger-scale air mass distribution around a TC.

[3]The effect of SAL, however, is likely more complex than providing a source of very dry air (e.g. Dunion and Velden, 2004).

ACPD
10, 28057–28107, 2010

1.2 Revisiting a horizontal and steady flow model

For steady, non-divergent flow the interaction of a vortex with the background flow gives rise to a dividing streamline that separates the area of rotation-dominated flow from the larger scale environment. Based on this simple fluid dynamical concept, Willoughby et al. (1984, hereafter WMF84) proposed that for a TC in storm-relative environmental flow "the streamline pattern is divided into a vortex core where the streamlines form a closed gyre and the vortex envelope where they curve around the core in a wavelike pattern" (Fig. 1). They noted further that "in the closed gyre, the air moves with the vortex; in the envelope, environmental air passes through the vortex and around the core". Willoughby et al. noted clearly the existence and importance of flow boundaries in the vicinity of a vertically sheared TC. They indicated also that the air within the closed gyre has generally higher θ_e values than outside of the gyre.

WMF84's seminal hypothesis of separated flow regions with distinct thermodynamic properties and its ramifications for the interaction of TCs with environmental air have received little attention in the literature since. WMF84's results are derived from a low wave-number analysis of observational data from a number of flight legs within 150 km of the storm center. Most notably, the stagnation point was not contained within the domain considered by WMF84. We believe that it is worthwhile to revisit WMF84's seminal hypothesis and analyze the flow topology of a TC in vertical wind shear with a much more complete data set from an idealized numerical experiment.

Consistent with WMF84's analysis we will assume that the environmental flow is layer-wise horizontal and steady. The first assumption is supported by scaling arguments for large-scale tropical circulations (Charney, 1963; Holton, 2004, Ch. 11) and is a good approximation outside of convective regions. The time scale of significant intensity modification during vertical shear interaction in our numerical experiment is 6 h–24 h, consistent with TCs in the real atmosphere (e.g. Zehr, 2003). Changes in the velocity field are usually small on this time scale and thus it is reasonable to assume the flow to be steady.

ACPD
10, 28057–28107, 2010

In the vicinity of the eyewall, however, both assumptions break down. In a mature TC, vortex Rossby waves (VRWs) and their coupling to convection and the boundary layer are arguably the most important transient flow features in this region (Montgomery and Kallenbach, 1997; Chen and Yau, 2001; Wang, 2002). For an intensifying TC, vortical hot towers can be expected to be dominant features (Nguyen et al., 2008). This rich dynamical behavior is not considered here. An extensive trajectory analysis of the time-dependent, three-dimensional flow to quantify the mid-level ventilation of eyewall convection in a numerical simulation of Hurricane Bonnie (1998) has been performed by Cram et al. (2007).

A natural extension of the current study is to examine the Lagrangian coherent structures (LCS) that govern the interaction of fluid from distinct regions in the unsteady, three-dimensional flow (e.g. Haller, 2001). First analyses of LCS in TCs have recently been performed by Sapsis and Haller (2009) and Rutherford et al. (2010). We anticipate that the analysis of LCS in a vertically sheared TC will yield further insight into the interaction of the TC with environmental air. The current study nonetheless should provide a useful framework for interpreting the results from an analysis of the LCS.

An outline for the paper is as follows. In Sect. 2 we present the flow topology and its relation to distinct air masses around the vertically sheared TC in our idealized numerical experiment. A simple analogue model based on a point vortex with singular mass sink is developed in Sect. 3. This model is shown to be able to explain the basic features of the flow topology in the idealized numerical experiment. Section 4 considers application of the analogue model to the problem of TC-environment interaction. Conclusions are presented in Sect. 5.

2 Flow topology in an idealized numerical experiment of TC – shear interaction

We analyze the flow topology of a mature TC in an idealized numerical experiment. The experiment analyzed herein is the 15mps case of RMN. The Regional Atmospheric Modeling System (RAMS, Pielke et al., 1992; Cotton et al., 2003) was used to perform

ACPD
10, 28057–28107, 2010

this experiment. We have deliberately employed a very simple set of parametrizations, most importantly a bulk aerodynamic formulation for the surface fluxes and warm-rain microphysics. For a detailed description of the RAMS and the experimental setup the reader is referred to RMN. Our experiment considers a TC that has been spun up in quiescent environment on an f-plane for 48 h. After this time the TC has reached an intensity[4] of 68 ms^{-1} and is suddenly exposed to a zonal wind profile with vertical shear. The zonal wind profile has a vertical, cosine structure with zero winds at the surface and 15 ms^{-1} easterlies at 12 km and above. After the environmental shear flow is imposed, the TC starts moving to the west, with a small southward component, with an average translation speed of 5 ms^{-1}.

Distinct changes in the TC structure occur a few hours after shear is imposed. The structural changes and their important connection to the thermodynamic impact on the TC inflow layer have been examined in detail in RMN. In response to the vertical shear forcing the TC vortex settles quickly into a quasi-equilibrium tilt direction left of the shear vector[5]. The vorticity anomaly associated with the tilt of the outer vortex at low levels contributes to the formation of a pronounced convective asymmetry outside of the eyewall, reminiscent of the stationary band complex (SBC) defined by WMF84. The SBC extends outwards up to a radius of approx. 180 km and wraps from the downshear-right at low levels to the downshear to downshear-left quadrants at upper levels. Strong and persistent, vortex-scale downdrafts form underneath the helical SBC updrafts. These downdrafts flush the inflow layer with low θ_e air in the downshear-left semicircle. RMN argue that, to first order, it is this flushing of the inflow layer with low θ_e that governs the intensity evolution of the vertically sheared TC. While the TC in the reference run without vertical wind shear continues to intensify rapidly, the intensity of the TC in the 15mps case remains approximately constant in the first 8 h–10 h after the shear is im-

[4] In RMN and in this study, intensity is defined as the maximum azimuthal mean tangential wind at 1 km height.

[5] In RMN, the tilt is defined as the vector difference between the location of the vorticity centroids at 10 km and 1 km height.

ACPD
10, 28057–28107, 2010

posed. With ongoing flushing of low θ_e air into the inflow layer, TC intensity decreases by 15 ms^{-1} in the subsequent 12 h.

2.1 Analyzed flow topology

The correct frame of reference is of immanent importance for the analysis of the flow topology under the assumption of steady flow (see, e.g., Fig. 3 of Dunkerton et al. (2009) and the accompanying discussion on pages 5624–5625). In our case, this is the frame of reference moving with the mature storm. We thus use data in a storm-relative frame of reference. A square domain of 2450 km side length centered on the TC[6] is considered, using data from the innermost grid (5 km resolution) where available and from the outer domains (15 km and 45 km resolution, respectively) elsewhere. Data is averaged over a 6 h period from 3 h–8 h after the shear was imposed. During this time, the structure and the intensity of the TC are approximately steady.

The flow topology is analyzed by calculating the streamlines that pass through the stagnation point. These streamlines constitute the hyperbolic manifolds of the flow, also referred to as separatrices (Ottino, 1989). If the flow were non-divergent, a closed streamline would emanate from the stagnation point, the so-called dividing streamline. The algorithm of Ide et al. (2002) is applied to linearize the velocity field in the vicinity of the stagnation point and to determine the location of the stagnation point. The stable (unstable) manifolds are found by forward (backward) integration of the steady, layer-wise horizontal velocity field, using a second-order Runge-Kutta scheme with a spatial increment of 2.5 km. The manifolds are seeded along the eigendirections of the linearized velocity field at a distance of 1 grid point (5 km) from the stagnation point.

[6]The center is defined as the centroid of vorticity averaged over the lowest 2 km in a square with a side length of 120 km around the surface pressure minimum.

ACPD
10, 28057–28107, 2010

2.1.1 Overview

We first provide an overview of the flow topology before examining its relation to the air mass distribution in the vicinity of the TC. The flow topology at low-levels above the inflow layer ($z = 2$ km), at mid-levels ($z = 5$ km), at upper-levels ($z = 8$ km), and just below the outflow layer ($z = 10$ km) will be considered in the following. The radial profiles of the azimuthally averaged tangential winds at these levels are shown in Fig. 2. As can be expected, the maximum tangential winds, as well as the tangential winds at outer radii, decrease with height. The shape of the radial profile is similar at all 4 levels.

The environmental storm-relative flow, calculated as the average storm-relative flow between radii of 200 km and 1000 km, is 4.5 ms^{-1} from 250° at 2 km, 1.5 ms^{-1} from 160° at 5 km, 6.5 ms^{-1} from 100° at 8 km, and 8 ms^{-1} from 95° at 10 km. The storm-relative flow changes sign between low- and upper-levels and is minimized at mid-level which is characteristic of a vertical shear profile with a vertical wave number 1 structure. The strength of the tangential flow and the magnitude of the storm-relative flow at 2 km height in our numerical experiment is comparable to one of the cases considered by WMF84 (Hurricane David (1979), their Fig. 2), except for the direction of the storm-relative flow. As mentioned in WMF84, the flow topology can be reoriented to adjust for this difference.

The flow topology in our experiment and its vertical structure are shown in Fig. 3. A comparison of the flow topology in our numerical experiment at 2 km height (Fig. 3a) with WMF84's results (Fig. 1) reveals some notable differences. The stagnation point is found at a radius of approx. 700 km in our case, considerably farther outside than hypothesized by WMF84. One separatrix spirals inwards because the flow is weakly convergent at this level. This separatrix ends in a so-called limit cycle, a closed streamline encompassing the strong updrafts in the inner core. In this case, the limit cycle is analogous to the closed streamline that encompasses the inner core and contains the 'vortex air' in WMF84's hypothesized flow topology. In contrast, the outer portion of the separatrices are located at a considerably larger radius. These difference can be expected to be less pronounced for less intense TCs (see Eq. (13) below).

ACPD
10, 28057–28107, 2010

At 5 km (Fig. 3b) and 8 km (Fig. 3c) height the vortex is weakly convergent as can be inferred from the inward spiraling separatrix. At 10 km height (Fig. 3d), the flow is very weakly *divergent* indicating the transition to the well developed outflow layer above (not shown). As can be expected for the weaker storm-relative flow at 5 km height, the stagnation point is located at a larger radius (approx. 1000 km) than at 2 km height. Consistent with storm-relative flow from the south, the stagnation point is located to the west. The inner core is encompassed by a large limit cycle of approx. 150 km–200 km radius. At 8 km and 10 km height, the stagnation points are located to the south and within 200 km–300 km from the center. It is curious that the flow at 8 km height exhibits 3 stagnation points. Again, the location of the stagnation points is consistent with the direction and the stronger magnitude of the storm-relative flow, and the weaker swirling winds at these levels as compared to 2 km and 5 km height. At 8 km height the limit cycle just encloses the eyewall updrafts. At 10 km height, the separatrices form a virtually closed streamline that contains the eyewall.

The analyzed flow topology is virtually identical when time averages from 2 h–7 h and 4 h–9 h, respectively, are used. The general characteristics of the flow topology shown in Fig. 3 are also found for the 6 h periods from 10 h–15 h and 16 h–21 h. The temporal differences in the details of the flow topology are discussed in Sect. 2.1.3.

2.1.2 The meso-scale environment of the eyewall

A zoomed-in version of Fig. 3, overlaid with θ_e (Bolton, 1980) at each respective height level, is shown in Fig. 4. A striking feature is that the distribution of θ_e is closely related to the flow topology above the inflow layer up to 10 km height (Figs. 4a–d). Air with the highest values of θ_e are contained within the limit cycle (2 km–8 km height) or within the effectively closed streamline at 10 km height.

At 2 km height a clear wave number 1 asymmetry in the θ_e distribution is found (Fig. 4a). Very low values of θ_e are found within a radius of 100 km south of the center. To the north of the center, high values of θ_e are found within the limit cycle and the innermost spiral, extending to a radius of 150 km. The relation between the θ_e

ACPD
10, 28057–28107, 2010

distribution and the flow topology strongly indicates that the storm-relative flow distorts the envelope of high θ_e values in the inner core region above the inflow layer at low levels. In contrast, at 5 km height the θ_e distribution in the inner core is approximately symmetric, consistent with the shape and location of the limit cycle at this level (Fig. 4b). At 8 km, the highest θ_e values outside of the eyewall are found southwest of the center, approximately bounded by the separatrices.

At 10 km, air with θ_e values of 342 K and lower appears to approach the TC from upshear. The closed streamline at this level, however, still protects the highest θ_e values in the eyewall. The vertical motion field indicates that updrafts within the SBC provide higher θ_e air from below that is then advected to the downshear side with the quasi-steady flow.

At upper-levels (8 km and 10 km), the dividing streamline barely encompasses the eyewall. This close approach of the separatrices to the eyewall indicates a potential "hot spot" for the interaction of the eyewall updrafts with environmental air. Note, however, that the highest θ_e values are well contained within the limit cycle. In particular, there is no indication that the eyewall "leaks", i.e. that high θ_e air is consistently transported downshear from out of the eyewall. Furthermore, from the perspective of the Carnot-cycle heat engine, the impact of ventilation on TC intensity is weighted by the difference between the outflow temperature and the temperature at the ventilation level. Ventilation at upper levels is thus not very effective in decreasing TC intensity (Tang and Emanuel, 2010b). In the following we therefore focus on the interaction of environmental air at low- to mid-levels.

2.1.3 Time consistency

The details of the flow topology exhibit some variability for the 6 h time averaged periods from 10 h–15 h and 16 h–21 h. For the sake of brevity we do not present the respective figures but provide a brief description of the salient features.

For the 6 h period from 10 h–15 h the separatrix spirals inwards very slowly at 2 km height and ends in a limit cycle that is larger than in Fig. 4a. This larger limit cycle

ACPD
10, 28057–28107, 2010

encompasses all of the θ_e air with values larger than 342 K. At 5 km height there is no stagnation point found within the domain under consideration. This is plausible because the steering level of the TC is expected to be around 5 km height. The storm-relative flow is small at this height and consequently the stagnation point located at a very large radius (Eq. 13). At 8 km height, two stagnation points are found, located in the same region as found 6 h earlier. Both separatrices emanating from these points spiral around the storm center once before reaching the limit cycle. At 10 km height, the flow is weakly convergent at this time. Three stagnation points are analyzed from which 2 separatrices spiral around the center. One separatrix reaches the limit cycle encompassing the eyewall directly while the other spirals around the center once before merging into the limit cycle. The outer separatrix encompasses the eyewall approx. 50 km further outside than from 3 h–8 h.

For the 6 h period from 16 h–21 h the separatrix structure at the individual levels is again very similar as during the period from 3 h–8 h, except at 5 km height. There, the separatrix spirals slowly inwards and merges into a limit cycle with a radius of approx. 60 km.

Although there is some variability in the details of the flow topology at different times, the close relationship between the general separatrix structure and the distribution of θ_e is verified at all time periods. Therefore, the assumption of steady flow appears to be justified and the interpretation of the flow topology in terms of distinct streamlines is physically meaningful.

2.2 Feeding of downdrafts by environmental air

As discussed in RMN, persistent, vortex-scale downdrafts form in the downshear to downshear-left quadrant where precipitation from the helical SBC updrafts falls into the unsaturated air below. Further insight into the formation of these downdrafts can be obtained by examining the flow topology. Figure 5 indicates that the majority of the downdrafts occur outside of the limit cycle in a region of very low θ_e air at 2 km height (see Fig. 4a).

ACPD
10, 28057–28107, 2010

The separatrix structure and θ_e distribution in Fig. 4a indicates that the downdraft region is continuously fed with very low θ_e air from the environment. This flow configuration appears to have two important ramifications. The *continuous* supply of dry, environmental air prevents the saturation of the air in the downdraft region due to the evaporation of precipitation. It is therefore plausible that the downdraft pattern may persist as a quasi-*steady* feature. Secondly, the flow pattern indicates that the environmental air reaches the downdraft region with very little thermodynamic modification. Evaporation of precipitation from the SBC may thus occur in *very dry* air, leading to the formation of *particularly vigorous* downdrafts and an associated pronounced depression of the boundary layer θ_e.

2.3 Origin of environmental air fed into downdrafts

The separatrices derived from the steady flow identify distinct flow regions and their interaction in the limit of long time scales. For the time scale relevant for TC-environment interaction of $\mathcal{O}$(1 day) only subregions of the flow domain will be involved in such interaction. The extent of these subregions depend on the structure and magnitude of the velocity field. To estimate the origin of the air that is fed into the region of persistent downdrafts we calculate backward trajectories of the steady flow. The backward trajectories are seeded at 2 km height along a line segment to the south of the storm center that approximates the central area of the downdraft region (Fig. 6). The color coding in Fig. 6 denotes where the air parcels are located at 3 h, 6 h, 9 h, ... before reaching the line segment.

Figure 6 illustrates that the source region of the environmental air that feeds the downdraft area exhibits a pronounced asymmetric, azimuthal wave number 1 structure. For the first 12 h, the air originates almost exclusively from the west and north of the model TC. Subsequently, air progressively reaches the downdraft region that has spiraled around the center once. Ultimately, this air has its origin west of the TC also, as can readily be inferred from the separatrix structure. For the first 24 h, the source region of air interacting with the downdraft region from the south and east of the center

ACPD
10, 28057–28107, 2010

is confined to a small radial area (approx. 150 km–200 km). This radial area is considerably smaller than indicated by the outer separatrix, which is located at a radius of approx. 300 km south and east of the center. The potential ramification of this pronounced asymmetry of the source region of environmental air on TC intensity will be discussed in Sect. 4.3.

3 A potential flow model for TC flow topology

Here we develop a simple analogue model that captures several principal features of the flow topology presented in the foregoing discussion based on the idealized experiment. Our analogue model is based on the well known properties of a point vortex (e.g. Lamb, 1945) immersed in background flow, with a relatively weak mass sink. The model is in the same spirit of Smith et al. (2000) who also used a point vortex model to elucidate certain aspects of a TC in vertical shear. To our knowledge, the simple model has not been considered previously to examine the interaction of TCs with their environment.

3.1 A convergent point vortex immersed in a uniform background flow

We first consider a mass sink that is co-located with the point vortex.

3.1.1 Streamfunction and wind components

Consider first a point vortex at the origin **0** with circulation Γ in a cylindrical polar coordinate system with position vector $\boldsymbol{x} = (r, \phi)$. The vertical vorticity is then given by

$$\zeta(\boldsymbol{x}) = \Gamma \delta(\boldsymbol{x}), \tag{1}$$

where $\delta(\boldsymbol{x})$ is the two-dimensional Dirac delta function. The well-known associated streamfunction in the horizontal plane is

$$\Psi_v(r, \phi) = \frac{\Gamma}{2\pi} \ln r, \tag{2}$$

and the tangential wind

ACPD
10, 28057–28107, 2010

$$v_v = \frac{\partial \Psi_v}{\partial r} = \frac{\Gamma}{2\pi r}, \tag{3}$$

with correspondingly zero radial wind.

Now, instead, consider a point mass sink of strength D at the origin. This mass sink has divergence

$$\mathrm{div}(\boldsymbol{x}) = D\delta(\boldsymbol{x}). \tag{4}$$

Because the flow associated with this mass sink is everywhere non-divergent save for this singularity, the following streamfunction can be defined[7]:

$$\Psi_{\mathrm{div}}(r,\phi) = \frac{D}{2\pi}\phi. \tag{5}$$

Because of our desire to readily visualize the flow, we prefer the use of a streamfunction over the velocity potential. The associated radial wind

$$u_{\mathrm{div}} = \frac{\partial \Psi_{\mathrm{div}}}{r\partial\phi} = \frac{D}{2\pi r}. \tag{6}$$

The tangential velocity is identically zero. Hereafter, we will absorb the 2π into the definitions of Γ and D, viz., $\Gamma^* = \Gamma/2\pi$ and $D^* = D/2\pi$, and drop the * notation.

Since the problem of a point vortex in uniform background flow is invariant under (static) rotation we are free to choose the direction of U. We choose the background flow to be zonal and define $\phi = 0$ to be south. Let positive U denote westerly flow. Cyclonic and outward flow with respect to the origin is defined to be positive. The streamfunction associated with the background flow is then

$$\Psi_{\mathrm{bg}}(r,\phi) = Ur\cos\phi \tag{7}$$

[7]The streamfunction is a multi-valued function for which the Riemann sheets connect at $0/2\pi$.

ACPD
10, 28057–28107, 2010

and the tangential and radial wind components, respectively, are given by

$$v_{bg} = U\cos\phi \tag{8}$$

and

$$u_{bg} = -U\sin\phi. \tag{9}$$

3.1.2 Total streamfunction and flow visualization

Because potential flow satisfies the linear Laplace equation $\nabla^2\Psi = 0$ outside of flow singularities we may superpose the individual solutions. The total streamfunction for a divergent point vortex at the origin immersed in uniform background flow is then:

$$\Psi(r,\phi) = \Psi_v + \Psi_{div} + \Psi_{bg} = \Gamma \ln r + D\phi + Ur\cos\phi. \tag{10}$$

It is clear from this equation that the term associated with the mass sink (Ψ_{div}) introduces a jump discontinuity[8] of magnitude $2\pi D$ when a streamline crosses the southern semi-axis at $0/2\pi$. The streamfunction is therefore multi-valued. Still, Eq. (10) is meaningful to represent the flow field because it is differentiable and thus the wind field is unique. The hyperbolic manifolds and the streamlines of the flow can be readily visualized when one contour line is chosen to pass through the stagnation point and a contour interval of $2\pi D$, or an integer fraction thereof, is used (Fig. 7).

3.2 "TC-like" vortex strength and mass sink

In this subsection we use observations and our idealized numerical experiment to give a range of values for Γ and D that best represent a TC in the point vortex framework.

[8]The structure of the equation for the velocity potential Φ of the combined flow is essentially the same and thus a likewise discontinuity occurs if Φ were used instead of Ψ to represent the mass source.

ACPD
10, 28057–28107, 2010

3.2.1 Tangential flow

The tangential wind of the point vortex decreases as r^{-1}. It is well known that the radial decrease of tangential winds in mature TCs, v_{TC}, outside of the radius of maximum winds (RMW) is generally less than r^{-1}. A reasonable estimate of this radial structure is

$$v_{TC} = I_0 r^{-\gamma}, \tag{11}$$

with γ ranging between 0.4 and 0.7 (Mallen et al., 2005, and references therein), and I_0 is a constant denoting the storm intensity. Much of the variability of γ is believed to be associated with the stage of the TC life cycle[9]. In general, the radial decay of v_{TC} is slowest for storms at minimal hurricane strength or weaker. The radial decrease of tangential winds is somewhat steeper at upper-levels (Mallen et al., 2005). Due to the different radial profiles it can be expected that the details of the flow topology of a point vortex and a TC in background flow vary accordingly.

To investigate the general flow topology of the simple model in the context of TC – environment interaction we believe that it is a reasonable choice to define the strength of the point vortex by its tangential winds at 150 km. As is shown below (Sect. 3.3.1) this radius lies in between the radius of the stagnation point and the closest approach of the dividing streamline to the vortex center, except for strong vortices. Therefore, this choice appears to be a good compromise between underestimating the winds at larger radii and overestimating them at small radii. Accordingly, the associated circulation of the point vortex will be denoted by Γ_{150}.

The circulation of several vortices is defined to represent different TC intensities by the following procedure. We specify the maximum wind speed according to the

[9]There is some variability of γ with radius also, consistent with the well-known fact that the inner and outer wind fields can develop rather independently (Weatherford and Gray, 1988).

ACPD
10, 28057–28107, 2010

National Hurricane Center (NHC) for a tropical depression[10], tropical storm, and category 1, category 3, and category 5 hurricanes (Table 1). The corresponding point vortices are referred to as TD, TS, Cat1, Cat3, and Cat5, respectively. The RMW is set to 35 km[11]. We use Eq. (11) with $\gamma = 0.55$ to calculate the tangential wind speed at 150 km. This wind speed is then used in Eq. (3) to calculate the circulation Γ_{150} for the individual vortex. Compared to the generic TC profile with $\gamma = 0.55$, the point vortex overestimates the winds at 50 km by 64% and underestimates the winds at 500 km by 42%. A comparison of the point vortex profile with the radial profile of the tangential winds in our numerical experiment is provided in Fig. 2.

To estimate whether environmental air may reach the eyewall, the overestimation of the tangential wind speed at the radius representing the eyewall is clearly problematic. For this estimate we consider the representation of the different TC categories by a modified circulation, Γ_{50}, also. To calculate Γ_{50}, the above procedure is repeated with the winds of the point vortex matched to the TC profile at a radius of 50 km, instead of 150 km. For the Γ_{50} vortices, the approach of environmental air is likely overestimated because of the steeper radial wind profile of the point vortex as compared to the TC profile. Below, Γ refers to Γ_{150} unless otherwise noted.

The circulation of the point vortex may represent a TC of specified intensity up to midlevels, around 5 km. At upper-levels the tangential winds are considerably weaker. In conjunction with the faster radial decay of the wind speed (see above) the closest approach of environmental air to the core region can be expected at upper-levels below the outflow layer, consistent with the numerical results presented in Sect. 2.

[10]There is no minimum wind speed requirement for the NHC to declare a tropical depression. Here we use a wind speed of 10 ms^{-1} to characterize a relatively weak closed circulation.

[11]This value underestimates the RMW for tropical depressions and potentially for tropical storms.

ACPD
10, 28057–28107, 2010

3.2.2 Radial flow

The radial profile of the radial wind above the inflow layer is more variable and less documented observationally than the radial profile of the tangential winds. In this study, we use data from our previously published idealized numerical experiments (i.e., the no_shear, 15mps, and 20mps case of RMN) to estimate values for D. We consider the temporal average from 4 h–9 h. For all three experiments the radial flow at 150 km is approx. 1 ms^{-1} which, according to Eq. (6), yields a value of $D = -1.5 \times 10^5\ m^2\ s^{-1}$ for the point vortex model. At 50 km, this value of D yields a radial inflow velocity of 3 m/s^{-1}.

It needs to be pointed out, however, that the radial profiles of the TC in the idealized numerical experiments are not consistent with a point mass sink. For all three experiments the radial inflow does *not* increase inside 150 km. In the no_shear and 15mps case a radial *outflow* of 5 ms^{-1} is found at 50 km. There is considerable uncertainty associated with our choice of D. Nevertheless, the results of our analysis will be shown below to be only weakly sensitive to the choice of D over a range of reasonable values.

3.3 Flow topology

Without loss of generality, we consider a cyclonic vortex ($\Gamma > 0$) in westerly background flow ($U > 0$).

3.3.1 Non-divergent point vortex

By definition, the stagnation point (r_{sp}, ϕ_{sp}) is found where both the tangential and radial flow components vanish. The radial flow for the non-divergent vortex vanishes everywhere. The radial component of the westerly background flow vanishes for $\phi = 0$ and $\phi = \pi$, i.e. due south and due north of the center (Eq. 9). For a cyclonic vortex in westerly background flow the stagnation point is located to the north[12], i.e. $\phi_{sp} = \pi$.

[12] In the Southern Hemisphere, the stagnation point is to the south.

ACPD
10, 28057–28107, 2010

The condition for the cancellation of the tangential flow is

$$v_v(r_{sp},\phi_{sp}) + v_{bg}(r_{sp},\phi_{sp}) = \frac{\Gamma}{r_{sp}} + U\cos\phi_{sp} = 0. \quad (12)$$

Using $\phi_{sp} = \pi$ in Eq. (12) gives the radius of the stagnation point

$$r_{sp} = \frac{\Gamma}{U}. \quad (13)$$

As to be expected, for a weaker vortex and stronger background flow the stagnation point is found closer to the center. For a "Cat1" vortex in 5 ms^{-1} background flow the stagnation point resides at 444 km.

The value of the streamfunction at the stagnation point is given by

$$\Psi(r_{sp},\phi_{sp}) = \Gamma\left(\ln\frac{\Gamma}{U} - 1\right). \quad (14)$$

The corresponding streamline that passes through the stagnation point is called the dividing streamline. The closest approach of the dividing streamline to the point vortex is located on the opposite side of the stagnation point, i.e. south of the vortex. The radius of this closest approach for the non-divergent vortex, R_{nd}, is found by equating the streamfunction south of the vortex ($\phi = 0$) to the value of the dividing streamline:

$$UR_{nd} + \Gamma\ln R_{nd} = \Gamma\left(\ln\frac{\Gamma}{U} - 1\right). \quad (15)$$

Equation (15) can be written as

$$\alpha + \ln\alpha = -1 \quad (16)$$

ACPD
10, 28057–28107, 2010

with $\alpha = R_{nd}U/\Gamma$. A solution to Eq. (16) can be found numerically[13]: $\alpha \approx 0.278$. Hence we can write

$$R_{nd} = \alpha \frac{\Gamma}{U} \tag{17}$$

or in terms of the radius of the stagnation point

$$R_{nd} = \alpha r_{sp}. \tag{18}$$

3.3.2 Point vortex with mass sink

We now obtain an expression for the stagnation point $\left(r_{sp}^{div}, \phi_{sp}^{div}\right)$ in the case of the divergent point vortex. Since the divergent flow does not project on the tangential flow, Eq. (12) still gives the condition for the cancellation of the tangential wind component. However, the condition for the cancellation of the radial wind components now is

$$\frac{D}{r_{sp}^{div}} - U \sin \phi_{sp}^{div} = 0. \tag{19}$$

Combining Eq. (12) with Eq. (19) yields:

$$\phi_{sp}^{div} = \arctan(-D/\Gamma). \tag{20}$$

Because the arc-tangent function returns values between $\pm\pi/2$, Eq. (20) is best regarded as the deviation from the stagnation point in the non-divergent case ($\arctan(-D/\Gamma) = 0$ for $D = 0$). The equation for the azimuth of the stagnation point in our case is then

$$\phi_{sp}^{div} = \pi + \Delta, \tag{21}$$

[13]We have used Newton's method with 0.2 as the initial guess and a convergence threshold of 10^{-4}. A formal solution to Eq. (16) is $\alpha = \mathcal{W}(e^{-1})$, with the Lambert W function $\mathcal{W}$. The value of $\mathcal{W}(e^{-1})$, however, cannot be given analytically (wikipedia.org/wiki/Lambert_W_function).

ACPD
10, 28057–28107, 2010

with $\Delta = \arctan(-D/\Gamma)$. The azimuthal shift relative to the non-divergent case is governed by the ratio D/Γ, which is usually small for TC-like vortices. Under the condition that $D/\Gamma \ll 1$ we may linearize Eq. (20) to yield

$$\Delta \approx -D/\Gamma. \tag{22}$$

It is interesting to note that the direction of the azimuthal shift depends only on the sign of D/Γ. For a convergent, cyclonic vortex ($D < 0$, $\Gamma > 0$), the stagnation point is shifted anticyclonically with respect to the non-divergent vortex. Usually, $|D/\Gamma| \approx 0.1$–0.2. Therefore, the azimuthal shift of the stagnation point is on the order of 5°–10°.

Inserting Eq. (21) into Eq. (12) yields

$$r_{\mathrm{sp}}^{\mathrm{div}} = \frac{\Gamma}{U\cos\Delta}, \tag{23}$$

which again can be linearized for small Δ:

$$r_{\mathrm{sp}}^{\mathrm{div}} = \frac{\Gamma}{U(1-\Delta^2+\ldots)}. \tag{24}$$

To first order, the radius of the stagnation point does not change when a small mass sink is introduced. To second order $r_{\mathrm{sp}}^{\mathrm{div}}$ increases over its non-divergent counterpart. The value for the streamfunction at the stagnation point

$$\Psi(r_{\mathrm{sp}}^{\mathrm{div}}, \phi_{\mathrm{sp}}^{\mathrm{div}}) = \Gamma\left(\ln\frac{\Gamma}{U\cos\Delta} - 1\right) + D(\pi + \Delta). \tag{25}$$

The above results show that the *location of the stagnation point is not sensitive* to the introduction of a mass sink that is small compared to the vortex strength. *Nevertheless, the flow topology changes fundamentally. Due to the mass sink the formerly closed streamline opens up. A direct pathway emerges through which environmental air can spiral towards the center (Fig. 7b).* We can estimate the width d of the opening as

ACPD
10, 28057–28107, 2010

follows. In the steady case, the inflow through this opening balances the mass sink. Due south of the center we can write

$$\int_{R_i}^{R_o} v(r)dr + 2\pi D = 0, \tag{26}$$

where R_i and R_o denote the radii of the inner and outer separatrix, respectively, and v the tangential flow. We may assume that the radial interval is centered on R_{nd}. The value of the integral is then $Ud + \Gamma \ln\left(\frac{R_{\mathrm{nd}}+d/2}{R_{\mathrm{nd}}-d/2}\right)$. Expanding the logarithm in a Taylor series and truncating at third order, Eq. (26) reads

$$\left(U + \frac{\Gamma}{R_{\mathrm{nd}}}\right) d + 2\pi D = 0, \tag{27}$$

Using Eq. (17) we find

$$d = -\frac{\alpha}{1+\alpha}\frac{2\pi D}{U}. \tag{28}$$

For the standard value $D = -1.5 \times 10^5$ m^{2}s^{-1} and $U = 5$ ms^{-1}, we find that $d \approx 40$ km. This value compares well with the width of the opening illustrated in Fig. 7b. A close agreement between the value derived from Eq. (28) and the actual width has been verified for reasonable values of U and D (not shown). It is interesting to note that within this good approximation (Eq. 28) the opening between the separatrices depends on U and D only. It does not depend on the circulation Γ of the vortex.

In comparison to the (closed) dividing streamline the presence of the mass sink causes the inward spiraling separatrix to move closer to the center. An estimate for this inward displacement is $d/2$. The closest approach of the inner separatrix in the divergent case, R_{div}, is then

$$R_{\mathrm{div}} = R_{\mathrm{nd}} - d/2. \tag{29}$$

Accordingly, an estimate for the closest approach of the outer separatrix

$$R_{\mathrm{div}}^{\mathrm{out}} = R_{\mathrm{nd}} + d/2. \tag{30}$$

ACPD
10, 28057–28107, 2010

3.4 Point vortex with "asymmetric" mass sink

We do not attempt to give the analytic solution for a point vortex with a mass sink displaced from the center. We note that this flow configuration is not a steady-state solution because the mass sink would tend to be advected by the swirling winds of the point vortex. We use this flow configuration as an ad-hoc explanation for the occurrence of the limit cycle found in the flow topology of the idealized model TC (Fig. 3a).

The asymmetric convergence at low-levels in our idealized numerical experiment is associated with the SBC (not shown). At 2 km height, the SBC is located approximately north of the center. The centroid of convergence upon averaging azimuthally over the northern semicircle is at 120 km. In the point vortex model the mass sink is therefore placed due north at 120 km radius.

For the special case of a mass sink located on the line segment between the origin and the stagnation point, the impact on the location of the stagnation point can be analyzed analytically. Let us denote the radial location of the mass sink as R_{asy}. By symmetry, the projection of the divergent flow on the tangential wind component vanishes at the stagnation point in this case and the condition for the cancellation of the tangential wind, Eq. (12), remains unaltered. Let $(r_{\mathrm{sp}}^{\mathrm{asy}}, \phi_{\mathrm{sp}}^{\mathrm{asy}})$ denote the location of the stagnation point. The condition for the cancellation of the radial flow components (Eq. 19) then reads

$$\frac{D}{(r_{\mathrm{sp}}^{\mathrm{asy}} - R_{\mathrm{asy}})} - U\sin(\phi_{\mathrm{sp}}^{\mathrm{asy}}) = 0, \tag{31}$$

which can be re-written as

$$\frac{D_{\mathrm{asy}}}{r_{\mathrm{sp}}^{\mathrm{asy}}} - U\sin(\phi_{\mathrm{sp}}^{\mathrm{asy}}) = 0 \tag{32}$$

ACPD
10, 28057–28107, 2010

where

$$D_{\text{asy}} = D \frac{r_{\text{sp}}^{\text{asy}}}{r_{\text{sp}}^{\text{asy}} - R_{\text{asy}}}. \tag{33}$$

From Eq. (22) we see that

$$\frac{\Delta_{\text{sp}}}{\Delta_{\text{sp}}^{\text{asy}}} = \frac{r_{\text{sp}}^{\text{asy}} - R_{\text{asy}}}{r_{\text{sp}}^{\text{asy}}} = 1 - \frac{R_{\text{asy}}}{r_{\text{sp}}^{\text{asy}}}. \tag{34}$$

The azimuthal shift of the stagnation point in the presence of an asymmetric mass sink is denoted by $\Delta_{\text{sp}}^{\text{asy}}$. For a radial displacement of the mass sink that is small compared to the radius of the stagnation point, the change in azimuth of the stagnation point is small. As we have seen before, the radius of the stagnation point does not change to first order. Accordingly, the general structure of the flow topology outside of the radius of the mass sink is not sensitive to its precise location or strength.

A numerical solution for the streamfunction is obtained by shifting the divergent streamfunction (Eq. 5) to the location of the mass sink and then adding to the non-divergent solution. The same algorithm (Ide et al., 2002) as used for the numerical experiment in Sect. 2 is applied to find the precise location of the stagnation point. From this solution, the value of the streamfunction at the stagnation point is then determined.

Figure 7c verifies that the location of the stagnation point and the structure of the separatrices is not sensitive to the displacement of the mass sink in the regime of TC-like point vortices (cf. Fig. 7b). Reminiscent of the limit cycle in the idealized experiment (cf. Fig. 3a), a closed streamline emerges radially just inwards of the asymmetric mass sink. In the case of the simple point vortex model, however, the inner separatrix spirals into the mass sink and does not end in the putative "limit cycle".

ACPD
10, 28057–28107, 2010

4 Application of the point vortex model to TC – environment interaction

The examination of the flow topology in the previous sections demonstrates that the potential of the storm-relative environmental flow to bring environmental air close to the TC center is considerably limited by the deflection of the swirling winds. We now use the simple point vortex model to estimate for which combinations of TC intensity and storm-relative flow pronounced environmental interaction may be expected.

To apply the point vortex model, we have to assume a generic TC structure and associated θ_e distribution above the boundary layer in quiescent environment (Fig. 8). Particularly high values of θ_e are contained within the eye and the surrounding eyewall. A typical radial scale of the eyewall is 50 km. The region adjacent to the eyewall is often dominated by pronounced rain band activity. A typical radial scale for this region might be related to the stagnation radius of radially propagating VRWs and is $\mathcal{O}$(150 km) (Chen and Yau, 2001). Rain bands mix high-θ_e air from the boundary layer into the mid- to upper troposphere, considerably increasing θ_e values in the free troposphere as compared to the synoptic scale environment. Beyond this region, there is likely a transition region where θ_e values are still higher than in the synoptic-scale environment. In this region, surface fluxes are enhanced due to the TC winds, which could trigger sporadic deep convection. Strong rain bands may extend into this region also, contributing to further moistening. Beyond this region, outside a radius of $\mathcal{O}$(250 km), we assume that the thermodynamic properties of the atmosphere above the inflow layer are no longer modified by the TC. Air originating in this region is hereafter referred to as "environmental air". We will consider the two regimes of environmental interaction discussed in the introduction: The direct interaction of environmental air with the eyewall and the interaction with rain bands.

The assumed θ_e distribution is based on the common notion that a TC in quiescent environment is embedded in a region of moist air, the "moist envelope" (Kimball (2006); Braun (2010), personal communication)[14]. Consistent with these studies, we have

[14]We could not clarify the origin of the term "moist envelope". The notion of a moist, meso-

ACPD
10, 28057–28107, 2010

chosen a typical radius for environmental air of $\mathcal{O}(250\,\mathrm{km})$. Our idealized numerical experiment generally supports the existence of a moist envelope, albeit of smaller radial extent (Fig. 4b). A radius of 250 km might therefore overestimate the extent of moist air around the TC. The tangential winds of the point vortex, on the other hand, decay more rapidly with radius than for a typical TC wind profile (Sect. 3.2.1). Thus, environmental air in the point vortex model may penetrate closer to the center than for a more realistic radial wind profile. The sharper radial decrease of the tangential winds may therefore compensate to some degree for the potential overestimation of the moist envelope.

4.1 An estimate of potential environmental interaction based on the location of the dividing streamline

A simple estimate of potential environmental interaction can be derived from the location of the dividing streamline. For now, we assume that for a vertically sheared TC the environmental air is located outside of the dividing streamline, as in WMF84. If the closest approach of the dividing streamline to the center is within the rain band (150 km) or eyewall (50 km) radius, then pronounced interaction with rain bands and eyewall convection, respectively, can be expected. The closest approach of the dividing streamline is given by Eq. (17).

We first note that Eq. (17) provides theoretical support for the hypothesis in RMN that the "character" of shear-TC interaction scales with the ratio of TC intensity and shear magnitude. Here, the shear magnitude is represented by the storm-relative flow U, as discussed in the introduction.

For a given U, the storm-relative flow that is necessary to move the dividing streamline to a specified radius R_{nd} increases linearly with Γ. For the range of values of Γ representing TC intensities from TD to Cat5, we find distinct scenarios of potential environmental interaction (Fig. 9). Direct eyewall interaction seems likely for the TD and

scale eyewall environment may originate from WMF84's result that the 'vortex air' is confined to the vicinity of the TC by the swirling winds.

ACPD
10, 28057–28107, 2010

TS vortices for storm-relative flow starting at ~3 ms^{-1}, while storm-relative flow well above 10 ms^{-1} is necessary to move the dividing streamline to a radius of 50 km for the Cat3 and Cat5 vortices. Estimating that the low-level storm-relative flow is approximately half of the wind difference between 850 hPa and 200 hPa, i.e. the deep-layer shear, it can be concluded that direct interaction of environmental air with the eyewall of TCs of tropical storm intensity and below is likely in weak to moderate deep-layer shear of 6 ms^{-1} and above. For mature TCs of category 3 or stronger, a direct interaction of environmental air with the eyewall is unlikely even in strong deep-layer shear of 20 ms^{-1}. Note that we have used Γ_{50} to derive this result. Due to the slower radial decay of the tangential winds in real TCs, these estimates are a lower bound of the required storm-relative flow. Using larger circulation values to represent the respective TC category, e.g. Γ_{150}, the differences between the weak and the strong TC categories are even more pronounced (not shown). For mature storms (category 3 and above), moderate to strong deep-layer shear is likely to promote pronounced interaction of environmental air with rain bands. Such interaction can produce persistent, vortex-scale downdrafts leading to a considerable weakening of the storm (Fig. 5 and RMN).

The results presented above suggest that it is not only the dynamic resiliency of a TC that increases with intensity (Jones, 1995; Reasor et al., 2004). The ability of a TC to isolate itself from adverse *thermodynamic* interaction with environmental air increases with intensity also. Very distinct scenarios of possible environmental interaction in vertical shear are indicated for values of U and Γ that represent realistic TC conditions in this simplified framework.

4.2 An improved estimate of potential environmental interaction: inward flow rate of environmental air

It is important to note that environmental air can reside *within* the dividing streamline also (e.g. Fig. 4a). Potential interaction with this environmental air is not accounted for by the estimate presented in the previous subsection. In our simple point vortex

ACPD
10, 28057–28107, 2010

framework, environmental air resides within the dividing streamline when the stagnation radius is beyond 250 km. For the Cat1 vortex, $r_{sp} > 250$ km for $U < 8.9\,\mathrm{ms}^{-1}$ (Eq. 13). Furthermore, the effect of weak convergence above the inflow layer has not been taken into account in Sect. 4.1.

We propose that the rate $\mathcal{F}_{env}$ by which environmental air is transported into the rain band or eyewall region provides an improved estimate for potential environmental interaction in our simple model. The volumetric flow rate $\mathcal{F}$ through an area bounded by a curve $\mathcal{L}$ and unit height

$$\mathcal{F} = \int_{\mathcal{L}} v_n dl, \tag{35}$$

where dl is a line segment of $\mathcal{L}$ and v_n is the flow normal to dl. The inflow rate of environmental air, $\mathcal{F}_{env}$, is determined from the streamlines that connect the environmental radius and the rain band and eyewall radius, respectively. Streamlines are calculated that emanate along the environmental radius $R_{env} = 250$ km with a constant azimuthal spacing $\Delta\phi = 3°$. We select a subset $\mathcal{S}_c$ of these streamlines that exhibit radial inflow at R_{env} and connect to the rain band (eyewall) radius without orbiting the center. The radial flow at radius r associated with the ith streamline of this subset is denoted by $u_{\mathcal{S}_c^i}(r)$. Due to mass conservation and the steadiness of the flow, $\mathcal{F}_{env}$ at the rain band (eyewall) radius equals the radial inflow rate at the environmental radius associated with $\mathcal{S}_c$:

$$\mathcal{F}_{env} = \sum_i u_{\mathcal{S}_c^i}(R_{env}) R_{env} \Delta\phi. \tag{36}$$

We exclude orbiting streamlines from our calculation because air parcels along such paths move inwards very slowly. It seems unreasonable to assume that the flow is approximately steady on this longer time scale. Air parcels that spiral through the rain band region towards the eyewall are likely to interact considerably with rain bands before reaching the eyewall. It can be assumed that this interaction moistens the environmental air considerably before eyewall interaction takes place. It is, however, an

ACPD
10, 28057–28107, 2010

open question if convection outside of the eyewall is indeed vigorous enough to protect the inner core from such slow approach of environmental air.

The values of $\mathcal{F}_{\text{env}}$, calculated from the point vortex with centered mass sink, are depicted in Fig. 10 for a large part of the phase space relevant for TCs. For comparison, the values of U and Γ for which the closest approach of the dividing streamlines is at the rain band and eyewall radius, respectively, are indicated also. The dividing streamline apparently gives a good estimate for the onset of potential environmental interaction. In general, low values of $\mathcal{F}_{\text{env}}$ are found for values of Γ and U for which the dividing streamline is outside of the rainband (Fig. 10a) and eyewall radius (Fig. 10b), respectively. It is clear that $\mathcal{F}_{\text{env}}$ increases with increasing U for a given circulation Γ. For eyewall interaction, the location of the dividing streamline denotes the onset of the inflow of environmental air extremely well (Fig. 10b). For the rain band region (Fig. 10a), potential environmental interaction is slightly underestimated for strong vortices. With this small caveat in mind, the phase space diagram of the dividing streamline location (Fig. 9) may be used as a first, simple guidance to estimate the propensity of TC – environment interaction.

4.3 A well defined source region of environmental air

As noted in Sect. 2.3 in the discussion of Fig. 6, the source region of environmental air interacting with a TC may exhibit a pronounced asymmetric, azimuthal wave number 1 structure. For a Cat3 vortex with $U = 5.1\ \text{ms}^{-1}$ the envelope of streamlines that connect the environment to the rain band radius are overlaid on the flow topology in Fig. 11. It is evident that the main source region of the environmental air that is transported into the rain band region is to the northwest of the storm. Westerly storm-relative flow at low levels indicates that such a TC would be in easterly vertical wind shear.

Now consider a region of very dry air to the southeast of the storm (shaded region in Fig. 11). Although some of this air is located within 200 km of the TC center, the interaction of the dry air with the TC is greatly limited in the easterly wind shear scenario depicted in Fig. 11: the dry air is located outside of the outer dividing streamline. If the

ACPD
10, 28057–28107, 2010

vertical wind shear were westerly, however, the low-level storm-relative flow would be from the east. The pattern of the flow topology would be rotated by 180° and would indicate a pronounced intrusion of the very unfavorable dry air masses into the TC circulation.

This brief discussion demonstrates that in the presence of moisture gradients the adverse impact of vertical wind shear on a TC may be sensitive to the direction of the shear. If the flow topology favors the interaction with particularly dry air masses, a more pronounced weakening of the TC can be expected as in comparison to a shear direction that favors interaction with relatively moist environmental air.

The interaction of TCs with the meridional gradient of planetary vorticity leads to the formation of broad-scale vorticity asymmetries, the so-called β-gyres. In quiescent environment, the flow associated with the β-gyres exhibits weak to moderate northwesterly vertical wind shear on a TC (e.g. Bender, 1997; Ritchie and Frank, 2007). Ritchie and Frank have hypothesized that this so-called β-shear adds linearly to the environmental vertical shear over the storm center. Thus, these authors have proposed that TCs should be less susceptible to easterly than to westerly environmental shear. Future work should test both hypotheses for the potential importance of the shear direction for TC intensity change, e.g. in an idealized modeling framework.

5 Conclusions

The flow topology of an idealized TC in vertical wind shear has been examined under the assumption of steady and layer-wise horizontal flow. Our results show that for an intense TC the stagnation point and the associated separatrices may be found at significantly larger radii than hypothesized by WMF84. The layer-wise horizontal flow is weakly convergent above the inflow layer and below the outflow layer (2 km–8 km height). The inner separatrix spirals inwards and ends in the limit cycle, a dividing streamline that encompasses the eyewall in our idealized experiment at all levels. The eyewall is therefore well protected from the environment in the steady and layer-wise

ACPD
10, 28057–28107, 2010

horizontal framework and interaction of the eyewall convection with environmental air is unlikely.

The TC's moist envelope, high θ_e air that surrounds the eyewall in the inner core, is strongly distorted by the storm-relative flow. At 2 km height the moist envelope is highly asymmetric with very low θ_e air within 100 km of the center to the downshear-left. To the downshear-right, high θ_e air extend to 150 km radius at this height. The shape of the moist envelope is closely related to the location and shape of the limit cycle with the highest θ_e air being contained within the limit cycle.

Strong and persistent downdrafts form outside of the low-level limit cycle where precipitation from the helical SBC updrafts falls into very dry environmental air. The steady supply of dry environmental air in this region promotes the persistence and amplitude of the downdraft pattern. In the first 12 h following the imposition of vertical shear, air from the north and west of the center (downshear and downshear right) feeds into the downdraft region. Subsequently, the downdraft region is fed also by air that wraps around the center from the east and south. Interaction with air from the east and the south, however, is limited to a small radius ($\mathcal{O}$(200 km)). This radius is even smaller than indicated by the location of the outer separatrix at $\mathcal{O}$(300 km). The source region of the downdraft air clearly depends on the direction of the low-level storm-relative environmental flow, and thus on the shear direction. In the presence of a pronounced environmental moisture gradient, vertical wind shear may thus promote or impede the interaction with dry environmental air, depending on the direction of the shear vector.

A simple kinematic model based on a weakly convergent point vortex in background flow has been presented. This simple model can explain several salient features of the flow topology in the numerical experiment. Assuming a generic distribution of air masses around the TC, the potential for environmental interaction has been quantified by the inflow rate of environmental air to the radius of rain band and eyewall interaction, respectively. The location of the dividing streamline provides a very simple, yet good approximation for the propensity of environmental interaction. The closest approach of the dividing streamline to the vortex center is proportional to the ratio of the

ACPD
10, 28057–28107, 2010

vortex strength and the storm-relative flow. Under the assumption that the low-level storm-relative flow is approximately half of the deep-layer shear, distinct scenarios of possible environmental interaction are indicated for the range of point vortices and background flows that represent typical conditions of TCs in vertical wind shear. Our results suggest that it is not only the dynamic resiliency of a TC that increases with intensity (Jones, 1995; Reasor et al., 2004). The ability of a TC to isolate itself from adverse thermodynamic interaction with dry environmental air increases considerably with intensity also.

Appendix A

Relative importance of *D* and *U* for environmental interaction

The representation of the weakly divergent flow above the TC inflow layer by a singular mass sink is associated with considerable uncertainty (see Sect. 3.2.2). The relative importance of the divergent and storm-relative environmental flow in forcing interaction with environmental air is not self-evident. On the one hand, the introduction of a mass sink inside the dividing streamline has a profound impact on the flow topology by opening up a pathway for environmental air to spiral towards the vortex center. On the other hand, the weakly divergent flow is usually much smaller than the storm-relative flow, except very close the to mass sink. The following discussion shows that a modification of the potential environmental interaction is dominated by variations in the storm-relative flow rather than by variations of the divergent flow. The general features of our results should thus hold true even in the light of the considerable uncertainty associated with the representation of the weakly divergent flow.

An estimate of the relative importance can be obtained by comparing the rate of change of the closest approach of the separatrix south of the vortex center, R_{div}, with

ACPD
10, 28057–28107, 2010

U and D:

$$\frac{\partial R_{\mathrm{div}}}{\partial U} = -\frac{\alpha}{U^2}\left(\Gamma + \frac{\pi}{1+\alpha}D\right) \tag{A1}$$

and

$$\frac{\partial R_{\mathrm{div}}}{\partial D} = \frac{\alpha}{U}\frac{\pi}{1+\alpha}, \tag{A2}$$

respectively. Dividing Eq. (A1) by (A2) and replacing the differentials by small finite changes Δ one obtains

$$\Delta D = -\frac{1+\alpha}{\pi\alpha} R_{\mathrm{div}}^{\mathrm{out}} \Delta U. \tag{A3}$$

We may assume a typical variation of the storm-relative flow of $\Delta U = 1\,\mathrm{ms}^{-1}$. To change the radius of the inner separatrix by the same amount, ΔD needs to be $-2.2\times10^5\,\mathrm{m}^2\,\mathrm{s}^{-1}$ and $-0.7\times10^5\,\mathrm{m}^2\,\mathrm{s}^{-1}$ at 150 km and 50 km, respectively. Here we have approximated $R_{\mathrm{div}}^{\mathrm{out}}$ by R_{div}, which underestimates the values of ΔD. The ΔD values correspond to a relative change of the standard value of $D = -1.5\times10^5\,\mathrm{m}^2\,\mathrm{s}^{-1}$ of 150% and 50%, respectively. The relative importance of the divergent flow increases with smaller R_{div}, consistent with stronger radial divergent flow at smaller radii. The large relative change of D as compared to a relatively small change of $\Delta U = 1\,\mathrm{ms}^{-1}$, however, shows that changes in the location of the inner separatrix are dominated by variations in the storm-relative flow rather than by variations of the divergent flow.

Considering $\mathcal{F}_{\mathrm{env}}$ over a range of values of U and D for specified Γ (not shown) confirms that the variation of R_{div} with U and D is indeed a good approximation for the relative importance of the weakly divergent and the storm-relative flow. When connecting streamlines orbit the center completely, however, $\mathcal{F}_{\mathrm{env}}$ is constrained by D alone. In this case, the inflow is confined in between the same streamline and, due to mass conservation, this inflow has to be balanced by the mass sink D. For slowly inward spiraling streamlines, however, our assumptions of steady and layer-wise horizontal flow are likely to break down, as discussed in Sect. 4.2.

ACPD
10, 28057–28107, 2010

Acknowledgements. This research was performed while the first author held a National Research Council Research Associateship Award at the Naval Postgraduate School. We acknowledge helpful discussions with Kerry Emanuel, Kayo Ide, and Scott Braun, and Michael Bell's thoughtful comments on an earlier version of this manuscript. This work is supported by NASA grant NNG09HG031, NFS grant ATM-0649946, NSF Cooperative Agreement ATM-0715426, and ONR grant N000014-03-1-0185.

References

Barnes, G. M., Zipser, E. J., Jorgensen, D., and Marks, F.: Mesoscale and convective structure of a hurricane rainband, J. Atmos. Sci., 40, 2125–2137, 1983. 28061

Bender, M. A.: The effect of relative flow on the asymmetric structure in the interior of hurricanes, J. Atmos. Sci., 54, 703–724, 1997. 28059, 28060, 28088

Black, M. L., Gamache, J. F., Marks, F. D., Samsury, C. E., and Willoughby, H. E.: Eastern Pacific Hurricanes Jimena of 1991 and Olivia of 1994: The effect of vertical shear on structure and intensity, Mon. Weather Rev., 130, 2291–2312, 2002. 28060

Bolton, D.: The computation of equivalent potential temperature, Mon. Weather Rev., 108, 1046–1053, 1980. 28067

Carr, L. E. and Williams, R. T.: Barotropic vortex stability to perturbations from axisymmetry, J. Atmos. Sci., 46, 3177–3191, 1989. 28060

Charney, J. G.: A note on large-scale motions in the tropics, J. Atmos. Sci., 20, 607–609, 1963. 28062

Chen, Y. and Yau, M. K.: Spiral bands in a simulated hurricane. Part I: Vortex Rossby wave verification, J. Atmos. Sci., 58, 2128–2145, 2001. 28063, 28083

Cotton, W. R., Pielke, R. A., Walko, R. L., Liston, G. E., Tremback, C. J., Jiang, H., McAnelly, R. L., Harrington, J. Y., Nicholls, M. E., Carrio, G. G., and McFadden, J. P.: RAMS 2001: Current status and future directions, Meteor. Atmos. Phys., 82, 5–29, 2003. 28063

Cram, T. A., Persing, J., Montgomery, M. T., and Braun, S. A.: A Lagrangian trajectory view on transport and mixing processes between the eye, eyewall, and environment using a high-resolution simulation of Hurricane Bonnie (1998), J. Atmos. Sci., 64, 1835–1856, 2007. 28063

ACPD

10, 28057–28107, 2010

Dunion, J. P. and Velden, C. S.: The impact of the Saharan air layer on Atlantic tropical cyclone activity, B. Am. Meteorol. Soc., 85, 353–365, 2004. 28061
Dunkerton, T. J., Montgomery, M. T., and Wang, Z.: Tropical cyclogenesis in a tropical wave critical layer: easterly waves, Atmos. Chem. Phys., 9, 5587–5646, doi:10.5194/acp-9-5587-2009, 2009. 28065
Emanuel, K., DesAutels, C., Holloway, C., and Korty, R.: Environmental control of tropical cyclone intensity, J. Atmos. Sci., 61, 843–858, 2004. 28059
Frank, W. M. and Ritchie, E. A.: Effects of vertical wind shear on the intensity and structure of numerically simulated hurricanes, Mon. Weather Rev., 129, 2249–2269, 2001. 28059
Haller, G.: Distinguished material surfaces and coherent structures in three-dimensional fluid flows, PHYSICA D, 149, 248–277, 2001. 28063
Holton, J.: An introduction to dynamic meteorology, AcademicPress, London, 4th edn., 2004. 28062
Houze, R. A., Cetrone, J., Brodzik, S. R., Chen, S. S., Zhao, W., Lee, W.-C., Moore, J. A., Stossmeister, G. J., Bell, M. M., and Rogers, R. F.: The hurricane rainband and intensity change experiment: Observations and modeling of Hurricanes Katrina, Ophelia, and Rita, B. Am. Meteorol. Soc., 87, 1503–1521, 2006. 28061
Ide, K., Small, D., and Wiggins, S.: Distinguished hyperbolic trajectories in time-dependent fluid flows: analytical and computational approach for velocity fields defined as data sets, Nonlin. Processes Geophys., 9, 237–263, doi:10.5194/npg-9-237-2002, 2002. 28065, 28082
Jones, S. C.: The evolution of vortices in vertical shear. I: Initially barotropic vortices, Q. J. Roy. Meteorol. Soc., 121, 821–851, 1995. 28085, 28090
Kimball, S. K.: A modeling study of hurricane landfall in a dry environment, Mon. Weather Rev., 134, 1901–1918, 2006. 28061, 28083
Lamb, H.: Hydrodynamics, Dover Publications, New York, 6th edn., 1945. 28071
Mallen, K. J., Montgomery, M. T., and Wang, B.: Reexamining the near-core radial structure of the tropical cyclone primary circulation: implications for vortex resiliency, J. Atmos. Sci., 62, 408–425, 2005. 28074
Marks, F. D., Houze, R. A., and Gamache, J. F.: Dual-aircraft investigation of the inner core of Hurricane Norbert. Part I: Kinematic structure, J. Atmos. Sci., 49, 919–942, 1992. 28059
Melander, M. V., McWilliams, J. C., and Zabusky, N. J.: Axisymmetrization and vorticity-gradient intensification of an isolated two-dimensional vortex through filamentation, J. Fluid Mech., 178, 137–159, 1987. 28060

ACPD
10, 28057–28107, 2010

Montgomery, M. T. and Kallenbach, R. J.: A theory for vortex Rossby-waves and its application to spiral bands and intensity changes in hurricanes, Q. J. Roy. Meteorol. Soc., 123, 435–465, 1997. 28063

Nguyen, S. V., Smith, R. K., and Montgomery, M. T.: Tropical-cyclone intensification and predictability in three dimensions, Q. J. Roy. Meteorol. Soc., 134, 563–582, 2008. 28063

Ottino, J. M.: The kinematics of mixing, stretching, chaos, and transport, Cambridge University Press, New York, 1989. 28065

Pielke, R. A., Cotton, W. R., Walko, R. L., Tremback, C. J., Lyons, W. A., Grasso, L. D., Nicholls, M. E., Moran, M. D., Wesley, D. A., Lee, T. J., and Copeland, J. H.: A comprehensive meteorological modeling system – RAMS, Meteor. Atmos. Phys., 49, 69–91, 1992. 28063

Powell, M. D.: Boundary layer structure and dynamics in outer hurricane rainbands. Part II: Downdraft modification and mixed layer recovery, Mon. Weather Rev., 118, 918–938, 1990. 28061

Reasor, P. D., Montgomery, M. T., and Grasso, L. D.: A new look at the problem of tropical cyclones in vertical shear flow: Vortex resiliency, J. Atmos. Sci., 61, 3–22, 2004. 28085, 28090

Riemer, M., Montgomery, M. T., and Nicholls, M. E.: A new paradigm for intensity modification of tropical cyclones: thermodynamic impact of vertical wind shear on the inflow layer, Atmos. Chem. Phys., 10, 3163–3188, doi:10.5194/acp-10-3163-2010, 2010. 28060

Ritchie, E. A. and Frank, W. M.: Interactions between simulated tropical cyclones and an environment with a variable Coriolis parameter, Mon. Weather Rev., 135, 1889–1905, 2007. 28088

Rutherford, B., Dangelmayr, G., and Montgomery, M. T.: Lagrangian coherent strutruces involved in vortical hot tower interaction, in preparation, 2010. 28063

Sapsis, T. and Haller, G.: Inertial particle dynamics in a hurricane, J. Atmos. Sci., 66, 2481–2492, 2009. 28063

Shelton, K. L. and Molinari, J.: Life of a six-hour hurricane, Mon. Weather Rev., 137, 51–67, 2009. 28059, 28060

Simpson, R. H. and Riehl, H.: Mid-tropospheric ventilation as a constraint on hurricane development and maintenance, in: Proc. Tech. Conf. on Hurricanes, D4.1—D4.10, Amer. Meteor. Soc., Miami, FL, 1958. 28059, 28060

Smith, R. K., Ulrich, W., and Sneddon, G.: On the dynamics of hurricane-like vortices in vertical-shear flows, Q. J. Roy. Meteorol. Soc., 126, 2653–2670, 2000. 28071

ACPD

10, 28057–28107, 2010

Tang, B. and Emanuel, K. A.: Midlevel ventilation's constraint on tropical cyclone intensity, J. Atmos. Sci., 67, 1817–1830, 2010a. 28059

Tang, B. and Emanuel, K. A.: Entropy ventilation in an axisymmetric tropical cyclone model, in: 29th Conference on Hurricanes and Tropical Meteorology, 7C.2, Amer. Meteor. Soc., Tucson, AZ, 2010b. 28068

Wang, Y.: Vortex Rossby waves in a numerically simulated tropical cyclone. Part I: Overall structure, potential vorticity, and kinetic energy budgets, J. Atmos. Sci., 59, 1213–1238, 2002. 28063

Weatherford, C. L. and Gray, W. M.: Typhoon structure as revealed by aircraft reconnaissance. Part II: Structural variability, Mon. Weather Rev., 116, 1044–1056, 1988. 28074

Willoughby, H. E., Marks, F. D., and Feinberg, R. J.: Stationary and moving convective bands in hurricanes, J. Atmos. Sci., 41, 3189–3211, 1984. 28059, 28060, 28062, 28097

Zehr, R. M.: Environmental vertical wind shear with Hurricane Bertha (1996), Weather Forecast, 18, 345–356, 2003. 28062

Zhang, D.-L. and Kieu, C. Q.: Potential vorticity diagnosis of a simulated hurricane. Part II: Quasi-balanced contributions to forced secondary circulations, J. Atmos. Sci., 63, 2898–2914, 2006. 28060

Zipser, E. J., Twohy, C. H., Tsay, S.-C., Thornhill, K. L., Tanelli, S., Ross, R., Krishnamurti, T. N., Ji, Q., Jenkins, G., Ismail, S., Hsu, N. C., Hood, R., Heymsfield, G. M., Heymsfield, A., Halverson, J., Goodman, H. M., Ferrare, R., Dunion, J. P., Douglas, M., Cifelli, R., Chen, G., Browell, E. V., and Anderson, B.: The Saharan air layer and the fate of African easterly waves: NASA's AMMA field study of tropical cyclogenesis, B. Am. Meteorol. Soc., 90, 1137–1156, 2009. 28061

ACPD

10, 28057–28107, 2010

Table 1. Definition of model vortices based on NHC TC intensity.

	TD	TS	Cat1	Cat3	Cat5
V_{NHC} [ms^{-1}]	10	17	33	50	70
Γ_{50} [$10^5 m^2 s^{-1}$]	4.1	7.0	13.6	20.5	28.8
Γ_{150} [$10^5 m^2 s^{-1}$]	6.7	11.5	22.2	33.7	47.2

ACPD
10, 28057–28107, 2010

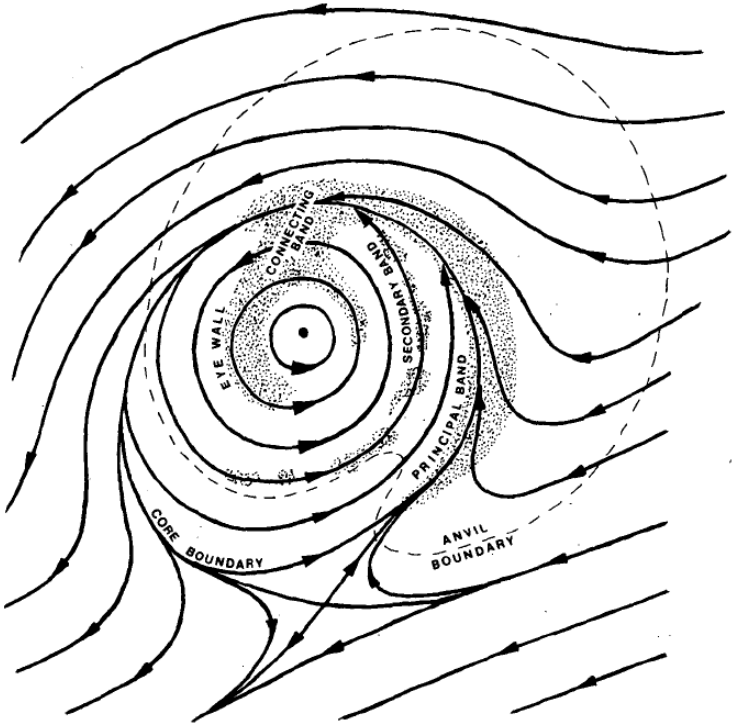

Fig. 1. Willoughby et al.'s hypothesized flow topology of a mature TC in northeasterly storm-relative environmental flow above the inflow layer (their Fig. 18). The closed gyre around the center is supposed to contain the moist "vortex air" while drier environmental air is found outside the dividing streamline.

ACPD
10, 28057–28107, 2010

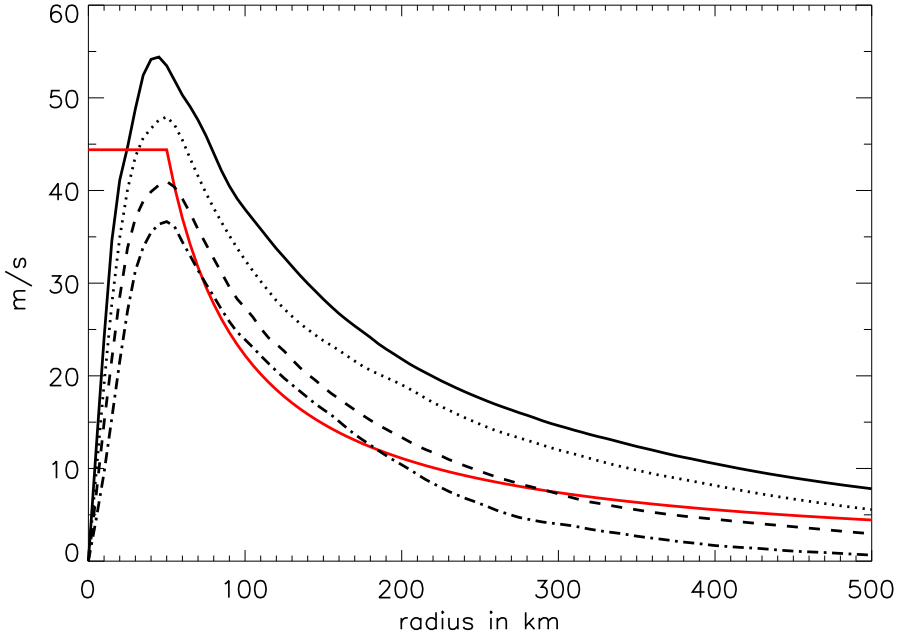

Fig. 2. Azimuthally averaged radial profiles of tangential winds for the no_shear case of RMN at 2 km (solid), 5 km (dotted), 8 km (dashed), and 10 km (dash-dotted), averaged over a 6 h period after 48 h of spin up. These profiles represent the TC wind structure at the time at which shear is imposed. For comparison, the profile for the Cat1 point vortex (red) is shown outside of 50 km.

ACPD
10, 28057–28107, 2010

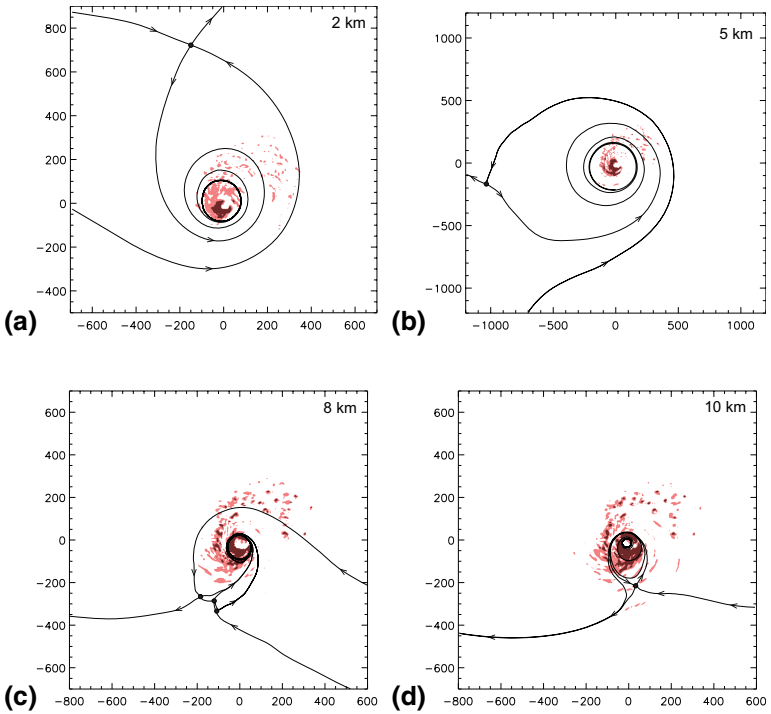

Fig. 3. Stagnation points (black dots) and separatrices at 2 km **(a)**, 5 km **(b)**, 8 km **(c)**, and 10 km **(d)** height. The eyewall updrafts are indicated by the dark red shading (1 ms $^{-1}$), light red shading denotes vertical motion of 0.25 ms^{-1}. The storm-relative flow is 4.5 ms^{-1} from 250° in (a), 1.5 ms^{-1} from 160° in (b), 6.5 ms^{-1} from 100° in (c), and 8 ms^{-1} from 95° in (d). 0° denotes north. The storm-relative flow is calculated as the averaged flow between 200 km and 1000 km radius. The values are rounded to 0.5 ms^{-1} and 5°, respectively. All fields are from the 15mps run of RMN and averaged from 3 h–8 h. The horizontal scale is in km; note the larger scale at 5 km height in (b). It is interesting to note that at 5 km height one branch of the unstable manifold does not extent away from the stagnation point. At 8 km height, 3 stagnation points are diagnosed.

ACPD
10, 28057–28107, 2010

Simple kinematic models for tropical cyclones

M. Riemer and
M. T. Montgomery

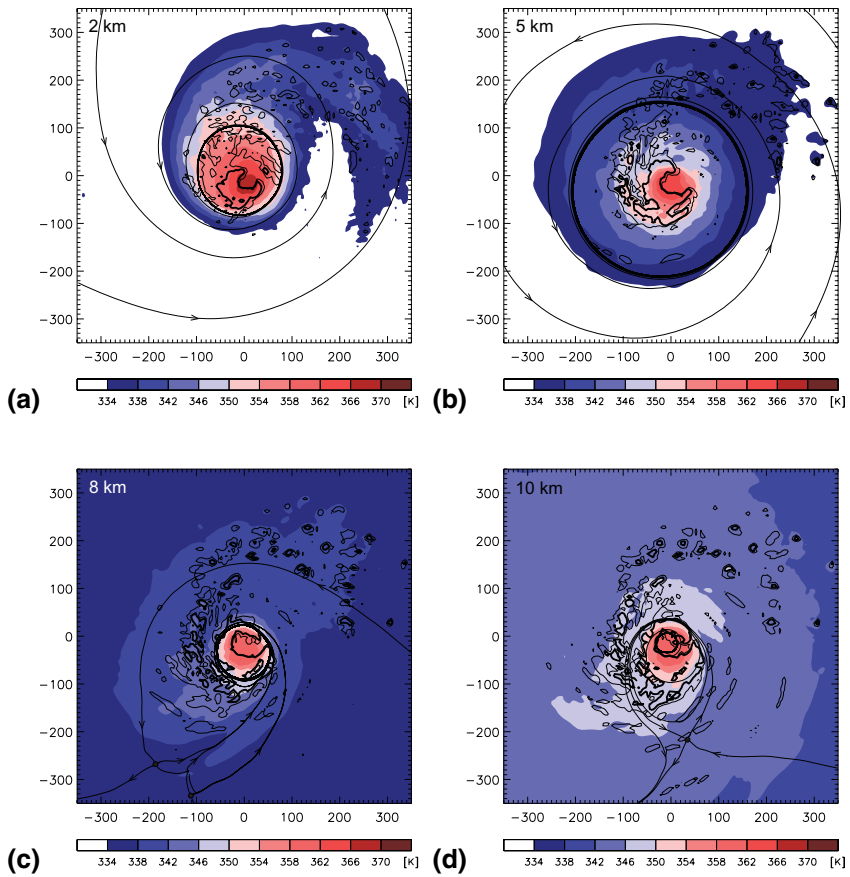

Fig. 4. Zoomed-in version of Fig. 3, including θ_e (color shaded) and vertical motion (thin contour = 0.25 ms^{-1}, thick contour = 1 ms^{-1}).

ACPD
10, 28057–28107, 2010

Simple kinematic models for tropical cyclones

M. Riemer and
M. T. Montgomery

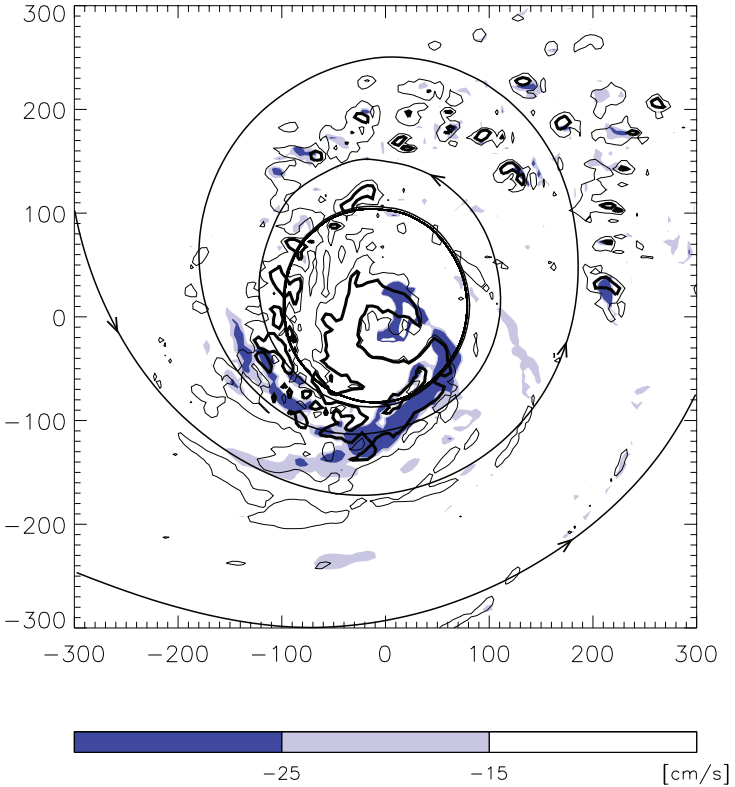

Fig. 5. Downdrafts (colored) and flow topology at 2 km and updrafts at 8 km (contours, thin = 0.25 ms^{-1}, thick = 1 ms^{-1}). Note that the limit cycle appears as a "thick contour" also because the manifold is plotted several times in a very similar location. The horizontal scale is in km.

ACPD
10, 28057–28107, 2010

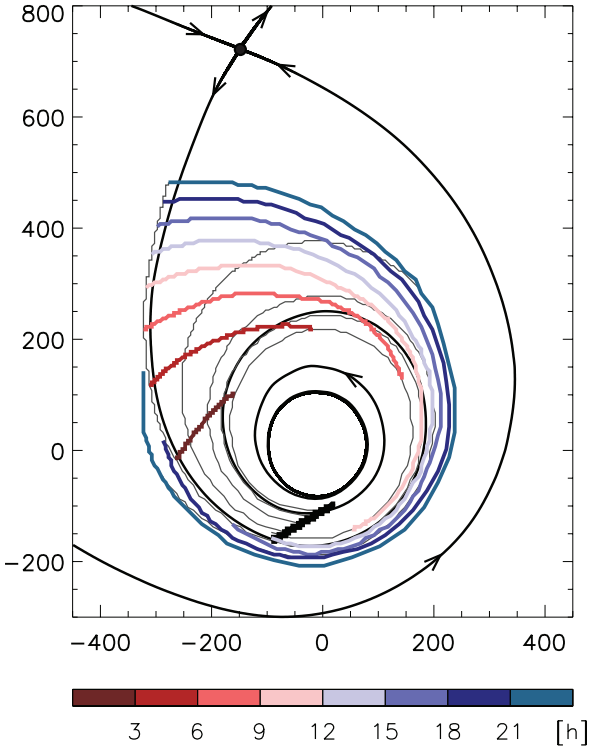

Fig. 6. Backward trajectories at 2 km seeded along a line segment (thick black line south of the center) approximating the central area of the downdraft region shown in Fig. 5. The colors denote the time it takes to reach the downdraft region. The gray lines exemplify some individual streamlines. The horizontal scale is in km.

ACPD
10, 28057–28107, 2010

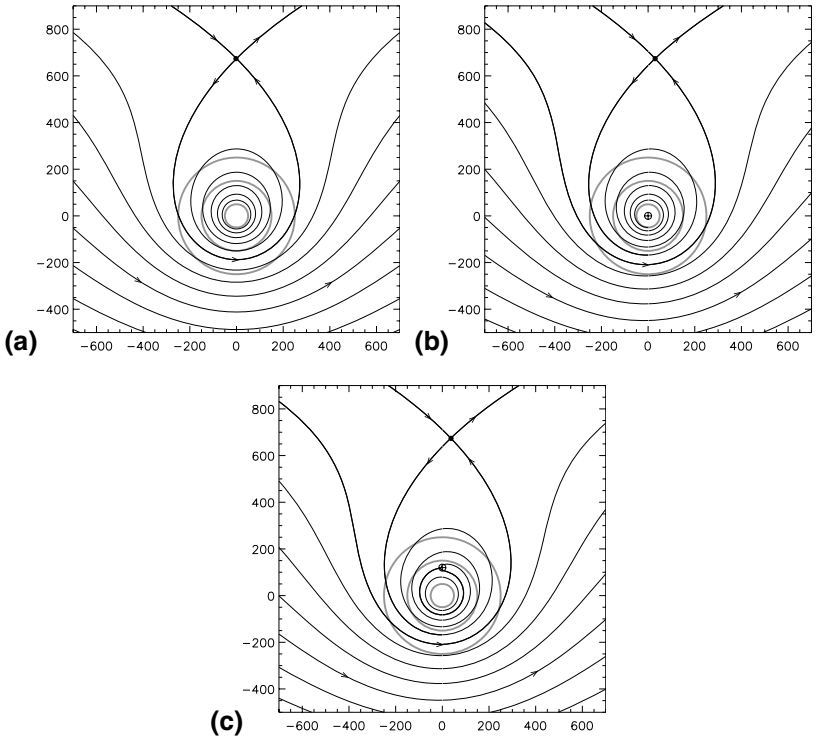

Fig. 7. **(a)** Streamlines of a stationary point vortex with a circulation of 33.7×10^{-5} m^2 s^{-1} (Cat3, see Table 1) in 5 ms^{-1} westerly background flow. The strength of the vortex and the storm-relative flow is similar as in the idealized numerical experiment at 2 km height (cf. Fig. 3a). The streamline passing through the stagnation point (black dot), the dividing streamline or so-called separatrix, is highlighted. The horizontal scale is in km. The gray rings denote radii 50 km, 150 km, and 250 km, respectively. **(b)** Same as (a) but for a weakly convergent point vortex with $D = -1.5\times10^{-5}$ m^2 s^{-1}. The mass sink is marked by the crossed circle. **(c)** Same as (b), but for a mass sink that is displaced 120 km to the north of the center. The emerging "limit cycle" is highlighted.

ACPD
10, 28057–28107, 2010

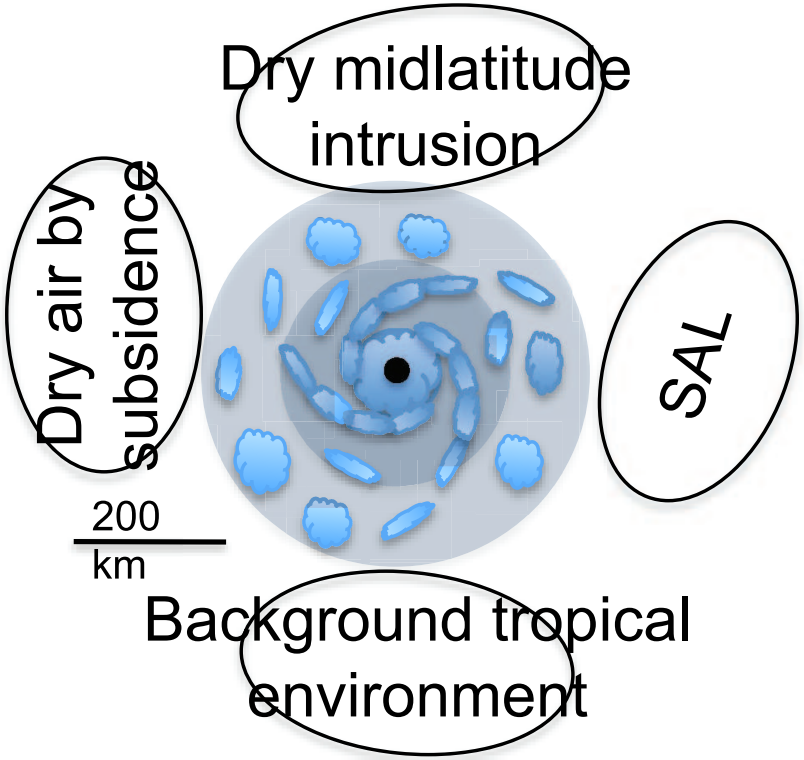

Fig. 8. Schematic of the generic structure of a TC in quiescent environment and possible environmental conditions. Gray shading indicates θ_e values, with darker shades denoting higher θ_e air (see text for details).

ACPD
10, 28057–28107, 2010

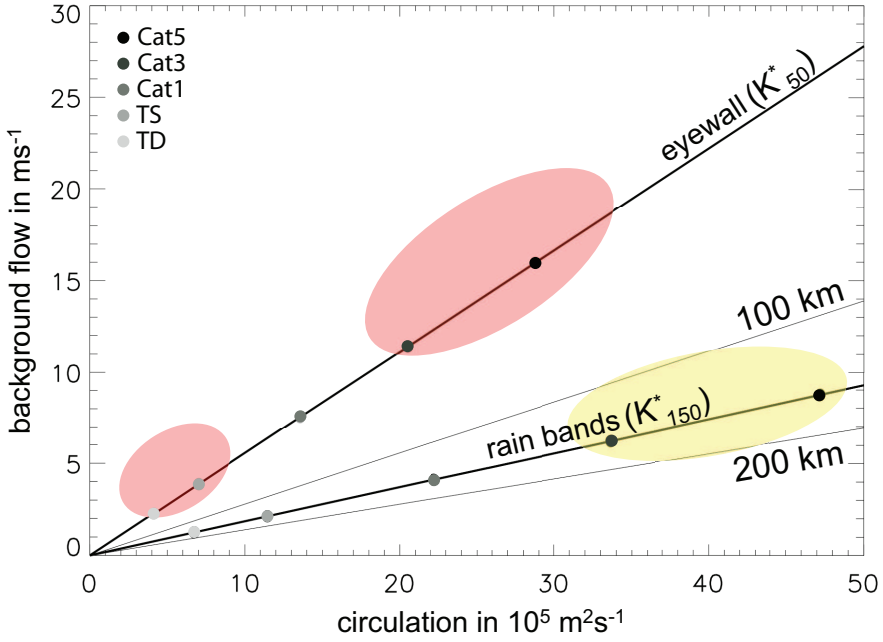

Fig. 9. The sloping lines denote the closest radius of the dividing streamline for a combination of circulation (abscissa) and storm-relative flow (ordinate). For eyewall interaction the TC categories are defined by Γ_{50}, for rain band interaction Γ_{150} is used (see Sect. 3.2.1). The TC categories are highlighted by the shaded dots. The red shading indicates the regime of eyewall interaction for weak and mature TCs (as defined in Table 1), respectively. Yellow shading indicates the regime of rain band interaction for mature TCs. The eyewall radius (50 km), 100 km, the rain band radius (150 km), and 200 km are depicted (from top to bottom).

ACPD
10, 28057–28107, 2010

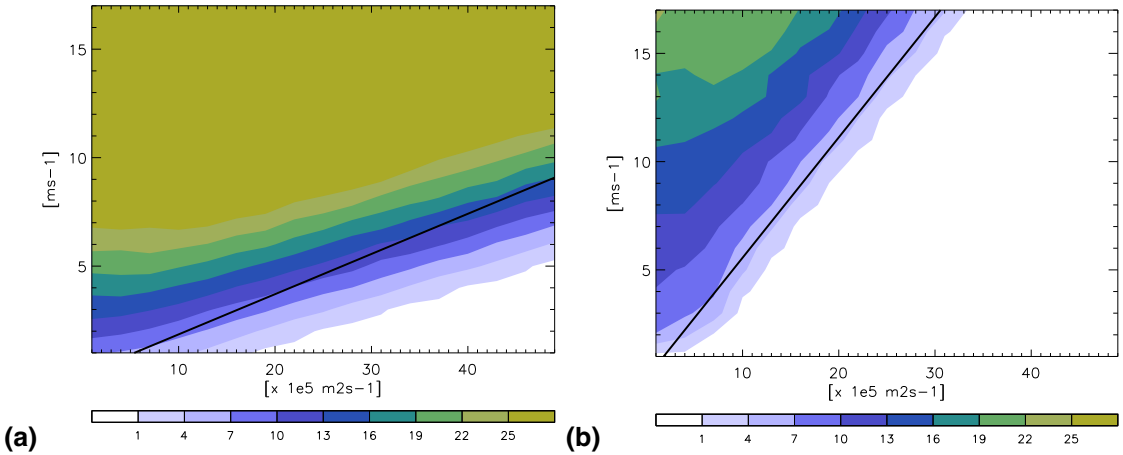

Fig. 10. Inflow rate of environmental air, $\mathcal{F}_{env}$ (in $10^5\,m^2\,s^{-1}$), at the radius of 150 km indicating rain band interaction **(a)** and at 50 km indicating eyewall interaction **(b)** as a function of circulation Γ (abscissa) and storm-relative flow U (ordinate). Values are calculated for the point vortex with centered mass sink ($D = -1.5 \times 10^{-5}\,m^2\,s^{-1}$). The solid line denotes the values of Γ and U for which the closest distance of the dividing streamline from the center is at the rain band (a) and eyewall (b) radius, respectively (cf. Fig. 9).

ACPD
10, 28057–28107, 2010

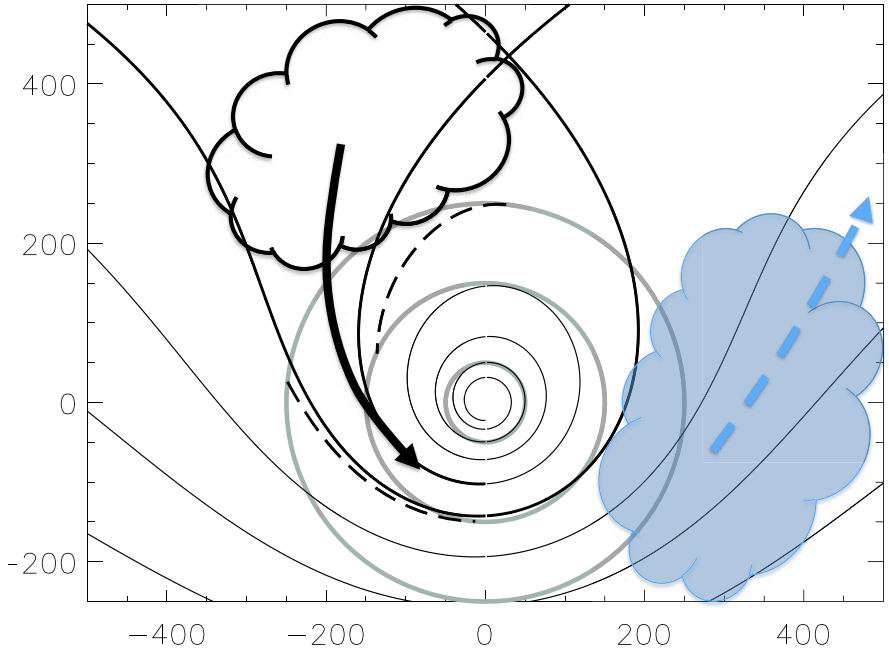

Fig. 11. Same as Fig. 7b, but for a Cat1 vortex in westerly storm-relative flow of $U = 5.1\,\mathrm{ms}^{-1}$. The dashed curves denote the outermost streamlines for which environmental air reaches the "rain band" region in this scenario. The source region of air that interacts with the TC is indicated to the northwest. The area shaded in blue indicates a hypothetical region of very dry environmental air.

ACPD
10, 28057–28107, 2010